Energy Advances

PAPER

View Article Online
View Journal | View Issue

Check for updates

Cite this: *Energy Adv.*, 2024, 3, 2367

Selective electroreduction of CO_2 into CO over Ag and Cu decorated carbon nanoflakes†

Ahmad Faraz,[a] Waheed Iqbal,[a] Shayan Gul,[a] Fehmida K. Kanodarwala,[b] Muhammad Nadeem Zafar,[cd] Guobao Xu *[de] and Muhammad Arif Nadeem *[ad]

Received 19th July 2024,
Accepted 26th July 2024

DOI: 10.1039/d4ya00462k

rsc.li/energy-advances

The electrocatalytic CO_2 reduction reaction (eCO_2RR) has the potential to effectively cut carbon emission. However, the activity and selectivity of eCO_2RR catalysts are topical due to the intricacy of the reaction components and mechanism. Herein, we have decorated silver and copper nanoparticles over carbon nanoflakes to achieve an Ag–Cu NPs/C system that enables selective reduction of CO_2 into CO. The catalyst is prepared by incorporating Ag nanoparticles into a Cu-BTC MOF (HKUST-1) and subsequent carbonization that alters the surface composition, with improved activity and faradaic efficiency (FE) towards selective CO_2 reduction. The evaluation of electrocatalytic performance reveals that the synthesized catalyst exhibits enhanced electrocatalytic activity and selectivity with a FE_{CO} of ~ 90% at −0.79 V_{RHE} and a current density (j) of 44.15 mA cm^{-2} compared to Ag-NPs and Cu/C. The durability test over 40 h confirms the outstanding stability of Ag–Cu NPs/C. The lower Tafel slope value of only 75 mV dec^{-1} corresponds to the fast reaction kinetics on the surface of Ag–Cu NPs/C. The synthetic protocol in this work offers an easy approach to the betterment of a cost-effective electrocatalyst with improved FE.

Introduction

Using carbon dioxide (CO_2) as an alternative source of fuel is one approach to reduce CO_2 emission and to provide a green source of energy.[1–4] The electrochemical CO_2 reduction reaction (eCO_2RR) is considered the most efficient technique[5] for the sustainable conversion of carbon dioxide into various valuable compounds[6,7] such as acids,[8] carbon monoxide (CO),[9] alcohols,[10] and hydrocarbons.[11,12] Carbon monoxide could be used as a starting material for the production of various useful chemicals.[13]

The eCO_2RR faces a few challenges including thermodynamic stability and kinetically inert nature of CO_2.[14–16] The conversion of CO_2 into CO also competes with the hydrogen evolution reaction (HER).[17] Therefore, development of highly selective and efficient eCO_2RR catalysts is a major challenge.[18,19] Many electrocatalysts, such as single-atom catalysts, metallic nanoparticles, metal organic frameworks (MOFs), covalent organic frameworks (COFs), and metal-free carbon based catalysts, have been utilized for the eCO_2RR to CO.[20–22] MOF derived carbon serves as an ideal support[23] due to its high surface area, porosity, thermal stability, and chemical stability.[24–26] In MOF derived nanomaterials, the inbuilt synergism between metallic nanoparticles dispersed over the carbon matrix results in improved catalytic performance.[27–29]

Recently, catalysts based on transition metals have been explored as CO_2 reduction catalysts.[30,31] Precious metals such as Au, Ag, and Pd are highly active in the eCO_2RR to CO but their high cost hinders the commercialization.[32–35] Thus, non-noble metal based catalysts are the topic of interest nowadays. The incorporation of non-noble metals into precious metal based catalysts reduces the cost and has the ability to enhance activity towards CO_2 reduction.[36,37] The intermediate (*COOH) binding strength during the conversion of CO_2 determines the effectiveness of the catalyst.[38] The catalyst with optimum binding strength can efficiently catalyze the cathodic CO_2 reduction.[39] According to the famous volcano plot, silver and copper possess weaker and stronger binding energies for *COOH, respectively.[40,41] The combination of copper and silver to obtain cost effective and efficient electrocatalysts with optimum binding strength can be a good choice.[42]

For example, Francesco *et al.* found that silver nanowires show a FE of 80% for CO at −1.4 V_{RHE}.[43] Mani *et al.* employed a molecular silver complex immobilized on graphitized mesoporous carbon for the eCO_2RR to CO and achieved a FE of 90%

[a] Department of Chemistry, Quaid-i-Azam University, Islamabad 45320, Pakistan. E-mail: manadeem@qau.edu.pk; Tel: +92-51-9064-2062
[b] University of Technology Sydney, NSW, 2007, Sydney, Australia
[c] Department of Chemistry, University of Gujrat, 50700, Gujrat, Pakistan
[d] State Key Laboratory of Electroanalytical Chemistry, Changchun Institute of Applied Chemistry, Chinese Academy of Sciences, Changchun, Jilin 130022, China. E-mail: guobaoxu@ciac.ac.cn
[e] School of Applied Chemistry and Engineering, University of Science and Technology of China, Hefei 230026, China

† Electronic supplementary information (ESI) available. See DOI: https://doi.org/10.1039/d4ya00462k

Open Access Article. Published on 06 August 2024. Downloaded on 1/20/2026 8:15:24 PM. This article is licensed under a Creative Commons Attribution-NonCommercial 3.0 Unported Licence.

Open Access Article. Published on 06 August 2024. Downloaded on 1/20/2026 8:15:24 PM. This article is licensed under a Creative Commons Attribution-NonCommercial 3.0 Unported Licence.

at −1.05 V_{RHE}.[44] Similarly, Yang *et al.* reported using oxide derived nanoporous silver for the conversion of CO_2 to CO and observed a faradaic efficiency of 87% at −0.8 V_{RHE}.[45] According to Zhipeng *et al.*, the formation of CO by using Cu/Ag(S) can achieve a FE of 90% and 2.9 mA cm^{-2} at −1.0 V_{RHE}.[46] Similarly Zekun *et al.* investigated the $Cu_{0.3}Zn_{9.7}$ electrocatalyst and revealed a FE of up to 90.69% for CO at −1.2 V_{RHE}.[47] Similarly, Cheng *et al.* proposed that the electrochemical reduction of CO_2 on the AgCu alloy facilitates C–C coupling kinetics, which retains a faradaic efficiency of 94 ± 4% towards multi-carbon products.[48] A. Harsh *et al.* found that the $Ag_{50}Cu_{50}$/p-Si catalyst converts CO_2 to CO and CH_4 with optimal faradaic efficiencies of 26% for CO and 18.2% at −0.72 V_{RHE} for CH_4.[49] Tao *et al.* reported that the Cu–Ag biphasic catalyst achieved a high FE_{CO} of 80.25% with a partial CO current density (j_{CO}) of −4.88 mA cm^{-2} at −0.9 V_{RHE}.[50] These reports further reveal that catalytic performance and properties can be tuned *via* alteration of surface components.[51]

In this work, we report an efficient eCO_2RR system using bimetallic silver and copper nanoparticles supported over carbon nanoflakes (Ag–Cu NPs/C), which was synthesized through pyrolysis of a composite, *i.e.* silver incorporated in a Cu-BTC MOF (HKUST-1), under reducing environment (H_2) in the high temperature range. HKUST-1 exhibits high stability, large pore size, high surface area, tunable structure, and cost effectiveness which make it a feasible choice to be used as a precursor for the synthesis of nanomaterials. The as-prepared catalyst performs better than conventional Ag or Cu based catalysts. Dispersion of silver and copper nanoparticles over carbon nanoflakes (Ag–Cu NPs/C) facilitates selective and active catalytic conversion of CO_2 to CO.

Experimental

Synthesis of the Cu-BTC MOF (HKUST-1)

A solvothermal approach, based on the existing procedure,[52] was used with minor modifications to synthesize the Cu-BTC MOF (HKUST-1). For this purpose, 400 mg of copper nitrate trihydrate was dissolved in 12 mL of a water:ethanol mixture followed by the addition of 246 mg of benzene-1,3,5-tricarboxylic acid. The above mixture was placed in a Teflon lined autoclave, which was placed in an oven at 120 °C for 12 h. The reaction mixture was allowed to cool to room temperature. The bluish green product was filtered, washed with water and ethanol, and dried in a vacuum oven for further use. The XRD pattern of HKUST-1 and the simulated pattern are shown in Fig. S1 (ESI†) which shows the successful synthesis of pure HKUST-1.

Synthesis of Ag@CuBTC

The synthesized Cu-BTC MOF was used to synthesize Ag@Cu-BTC. For this purpose, 600 mg of the thermally evacuated HKUST-1 MOF was dispersed in ethylene glycol and sonicated for an hour. 250 mg of polyvinylpyrrolidone (PVP) and 400 mg of $AgNO_3$ were then added to this suspension and subsequently refluxed for 2 h at 160 °C. After cooling, the product was filtered, washed with ethanol and water mixture, and dried in a vacuum oven.

Synthesis of Ag–Cu NPs/C

The weighed amount of Ag@CuBTC was placed in a tube furnace which was heated at various set temperatures under a hydrogen atmosphere. Ag–Cu NPs/C was formed during the carbonization of the composite, which was done for six hours in a reducing environment (H_2) at various temperatures, including 550 °C, 600 °C, 700 °C, and 850 °C, with a ramping rate of 10 °C min^{-1} (Scheme 1). For comparison, Ag-NPs and Cu/C were also synthesized by following this method.

Electrochemical measurements

Electrochemical measurements were used to estimate the prepared material's capacity to reduce CO_2. Using a GAMRY E-5000, all electrochemical investigations were carried out at ambient temperature. The eCO_2RR was evaluated in a gas tight H-type cell configured with a three-electrode system. This system featured anodic and cathodic compartments partitioned by a proton exchange membrane (PEM; Nafion 117). The drop-casting method was used to prepare working electrodes. For uniform mixing, a solution of 5 mg synthesized catalyst, 1 mL ethanol, and 20 μL of Nafion solution was sonicated for 3 h in a water bath. This homogenized slurry was applied uniformly onto a 1 cm^2 fluorine doped tin oxide (FTO) electrode. The coated electrodes were given

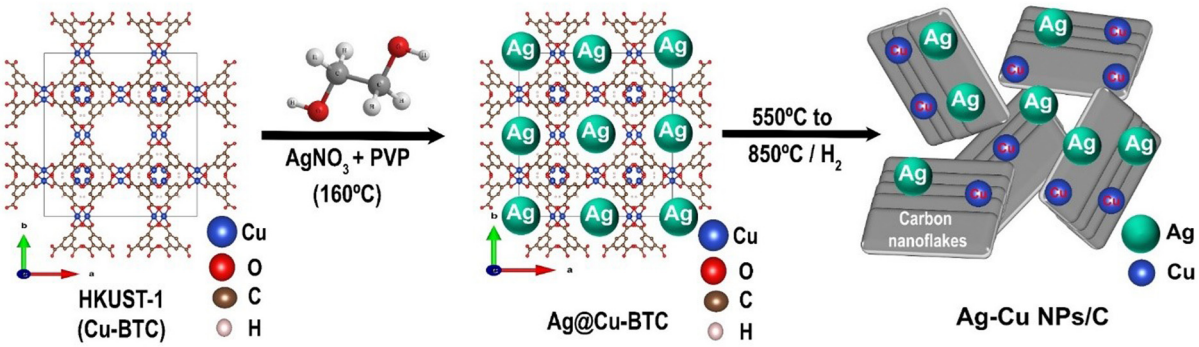

Scheme 1 Graphical illustration of the synthesis of Ag–Cu NPs/C.

© 2024 The Author(s). Published by the Royal Society of Chemistry

Open Access Article. Published on 06 August 2024. Downloaded on 1/20/2026 8:15:24 PM. This article is licensed under a Creative Commons Attribution-NonCommercial 3.0 Unported Licence.

their appropriate names after being dried for the whole night at 70 °C in an oven. The prepared catalyst on FTO acted as a working electrode where the CO_2 reduction occurs. The counter electrode used in this experiment was a graphite rod; the reference electrode was Ag/AgCl; and the electrolyte was 0.1 M $KHCO_3$. Before performing each electrochemical experiment, the electrolyte was degassed by purging high-purity argon for at least 30 min and then saturated with carbon dioxide. The Nernst equation used for converting potential values from Ag/AgCl to a standard RHE is as follows:

$$E_{RHE} = E_{Ag/AgCl} + 0.0592(pH) + 0.1976$$

where 0.0592 is equivalent to a factor $\frac{RT}{nF}$; 0.1976 = E° (standard electrode potential of Ag/AgCl).

Quantification of the products

The gaseous products of the eCO_2RR including CO and H_2 were identified by using gas chromatography equipped with a capillary column of Stabil wax (30 m × 0.32 mm I.D.), a 5 μm thick film, and a TCD detector. The Faraday efficiency for CO is calculated by using the following formula, given below.

$$FE_{CO} = \frac{\left(n_{CO(g)} + n_{CO(dissolved)}\right) \times n \times F}{I \times t} \times 100\%$$

where FE_{CO} indicates the Faraday efficiency of CO, n denotes the number of electrons transferred *i.e.*, for CO, n is equal to 2, $n_{CO(g)}$ is the quantity of CO in the headspace, and $n_{CO(dissloved)}$ is the quantity of CO dissolved in the electrolyte; it has a value of 1.774×10^{-5} and is calculated based on Henry's law; F represents the faradaic constant whose value is 96 485 C mol^{-1}, I is the total current in amperes (A), and t is the reaction time in seconds (s).

Results and discussion

Powder X-ray diffraction (PXRD) patterns of all the as-prepared materials are presented in Fig. 1(a) and it can be observed from the graph that the XRD spectra of Ag–Cu NPs/C reflect the characteristic peaks of Ag, at 2θ of (38.2°, 44.5°, 64.7°, and 77.7°) and Cu at 2θ of (43.39°, 50.49°, and 74.13°) corresponding to the crystalline planes of Ag (111) (200) (220) (311) and Cu (111) (200) (220), respectively. The diffraction peak at *ca.* 25° represents the crystal face of porous carbon, as depicted in Fig. S2(a) and (b) (ESI†). The distinct peaks of Ag and Cu match with the standard Ag card (JCPDS no. 03-065-2871) and Cu (JCPDS no. 00-003-1005). All the diffraction peaks correspond to metallic silver, copper, and carbon, and no other impurities can be detected.

X-ray photoelectron spectroscopy (XPS) was utilized to examine the electronic properties and the elemental composition of the surface of the Ag–Cu NPs/C catalyst. The XPS spectra obtained for Ag–Cu NPs/C are illustrated in Fig. 1(b)–(d). After careful analysis of the spectra, peaks associated with the elements Ag, Cu, and C were recognized. The Ag 3d and Cu 2p high-resolution scans from Ag–Cu NPs/C are shown in Fig. 1(b) and (c), respectively. The two prominent peaks of Ag 3d noticed at 368.2 eV and 374.2 eV are due to Ag $3d_{5/2}$ and Ag $3d_{3/2}$ of the Ag^0, respectively (Fig. 1(b)). The high-resolution profile of Cu 2p reveals the presence of two characteristic peaks at 932.8 eV and 953.0 eV attributed to Cu $2p_{3/2}$ and Cu $2p_{1/2}$, respectively (Fig. 1(c)). These peaks represent the formation of copper nanoparticles. The C 1s XPS spectra of Ag–Cu NPs/C are displayed in Fig. 1(d), with the peaks at binding energies of 284.8 eV and 284.5 given to the C–C bond and C=C, respectively. The presence of silver and copper peaks implies the successful incorporation of bimetallic nanoparticles into carbon nanoflakes.

Transmission electron microscopy (TEM) analysis is a promising technique for characterizing the morphology and structure of materials at the nanoscale. The TEM images of bimetallic silver nanoparticles incorporated into carbon in the form of nanoflakes (C) depict the unique morphology of the catalyst material and the distribution of silver and copper NPs throughout the carbon nanoflake support. In contrast, the catalyst material was synthesized through the pyrolysis of the Ag@Cu-BTC MOF, which gives it distinct morphological features with fully exposed nanoflakes like structures illustrated in Fig. 1(e)–(g). It represents metallic particles with an almost spherical shape, and the calculated lattice fringes *d*-spacing is 0.344 nm. The sizes of the metallic particles are determined by HRTEM and fall within the range of 10 nm to 40 nm. The high efficiency and selectivity of synthesized electrocatalysts may be attributed to the specific porous, nanoflakes of carbon and the synergistic effect of smaller sized Ag–Cu nanoparticles. The individual spherical nanoparticles can be seen for Ag–Cu NPs/C, which confirms the successful formation of both silver and copper nanoparticles that are dispersed over carbon nanoflakes. As shown in Fig. 1(e)–(g), various structures of NPs have been produced; however, the two discrete spherical dark and black contrasting TEM images made it challenging to distinguish between Ag and Cu nanocomponents. The confirmation of elements and surface quantification was also confirmed by EDX analyses (Fig. S6, ESI†). The actual ratio of Ag and Cu in the optimized catalyst is 1 : 0.75 as confirmed by edx and ICP techniques.

Electrochemical studies of Ag–Cu NPs/C

Linear sweep voltammetry (LSV) was used to examine the material's ability to function as an electrode for the reduction of CO_2. In 0.1 M $KHCO_3$ solution saturated with Ar and CO_2, Ag–Cu NPs/C (850 °C) was analyzed at a rate of 10 mV s^{-1} within a potential window of 0 to (−1.5 V) *vs.* Ag/AgCl. In CO_2 saturated solution, the LSV results of Ag–Cu NPs/C show better current density (j) and lower overpotential (η) than those of the Ar saturated medium (Fig. 2(a)). To gain a better understanding, an investigation of the eCO_2RR was carried out for Ag-NPs, Cu/C, and Ag–Cu NPs/C (Fig. 2(b)). The LSV results of Ag–Cu NPs/C exhibit low η and significantly improved j response for CO_2 reduction than those of Ag-NPs and Cu/C, confirming the higher activity of Ag–Cu NPs/C. A comparative LSV profile of

Open Access Article. Published on 06 August 2024. Downloaded on 1/20/2026 8:15:24 PM.
This article is licensed under a Creative Commons Attribution-NonCommercial 3.0 Unported Licence.

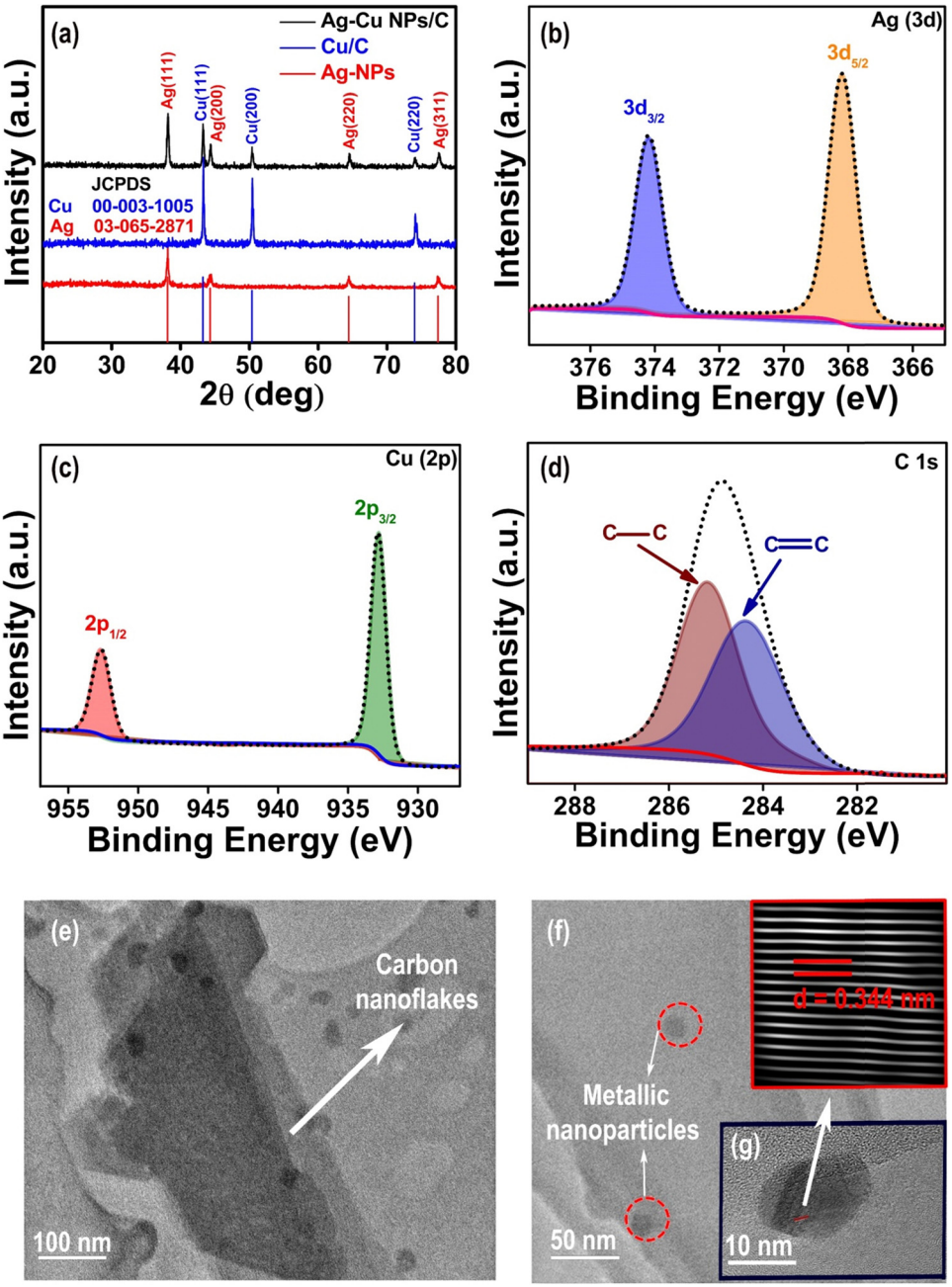

Fig. 1 Comparative PXRD patterns of Ag-NPs (red), Cu/C (blue), and Ag–Cu NPs/C (black) along with their JCPDS. XPS data of Ag–Cu NPs/C (b), Ag 3d (c) and Cu 2p (d) C1s. (e)–(g) TEM images of Ag–Cu NPs/C at different resolutions (100 nm, 50 nm, and 10 nm).

Ag–Cu NPs/C, which was synthesized by calcination under a reducing environment at different temperatures of 550 °C, 600 °C, 700 °C and 850 °C, reveals the catalytic activity in a CO_2-saturated medium. The recorded j for the electrocatalysts follows in this order: Ag–Cu NPs/C 550 °C (17.22 mA cm^{-2}) < Ag–Cu NPs/C 600 °C (20.1 mA cm^{-2}) < Ag–Cu NPs/C 700 °C (25.02 mA cm^{-2}) < Ag–Cu NPs/C 850 °C (44.14 mA cm^{-2}) (as illustrated in Fig. 2(c)). It appears that catalytic activity is found to enhance with an increase in carbonization temperature. The maximum catalytic activity is achieved for Ag–Cu NPs/C (850 °C), with a low onset potential of 0.430 V_{RHE} and a maximum j of 44.14 mA cm^{-2}. This indicates that with the increase in temperature, the particle size decreases and per unit active surface area increases. This in turn enhances CO_2 adsorption and the kinetics of the eCO_2RR. Fig. 2(d) demonstrates the partial CO current density (j_{CO}) for all synthesized electrocatalysts, notably Ag–Cu NPs/C 850 °C exhibits superior activity in the eCO_2RR over all the remaining synthesized electrocatalysts.

The electrochemical impedance spectroscopy (EIS) experiment depicted in Fig. 2(e) was conducted within the frequency limits of 0.01 Hz to 10^3 kHz to investigate the overall charge transfer resistance in the circuit. The spectra obtained by

© 2024 The Author(s). Published by the Royal Society of Chemistry

Open Access Article. Published on 06 August 2024. Downloaded on 1/20/2026 8:15:24 PM.
This article is licensed under a Creative Commons Attribution-NonCommercial 3.0 Unported Licence.

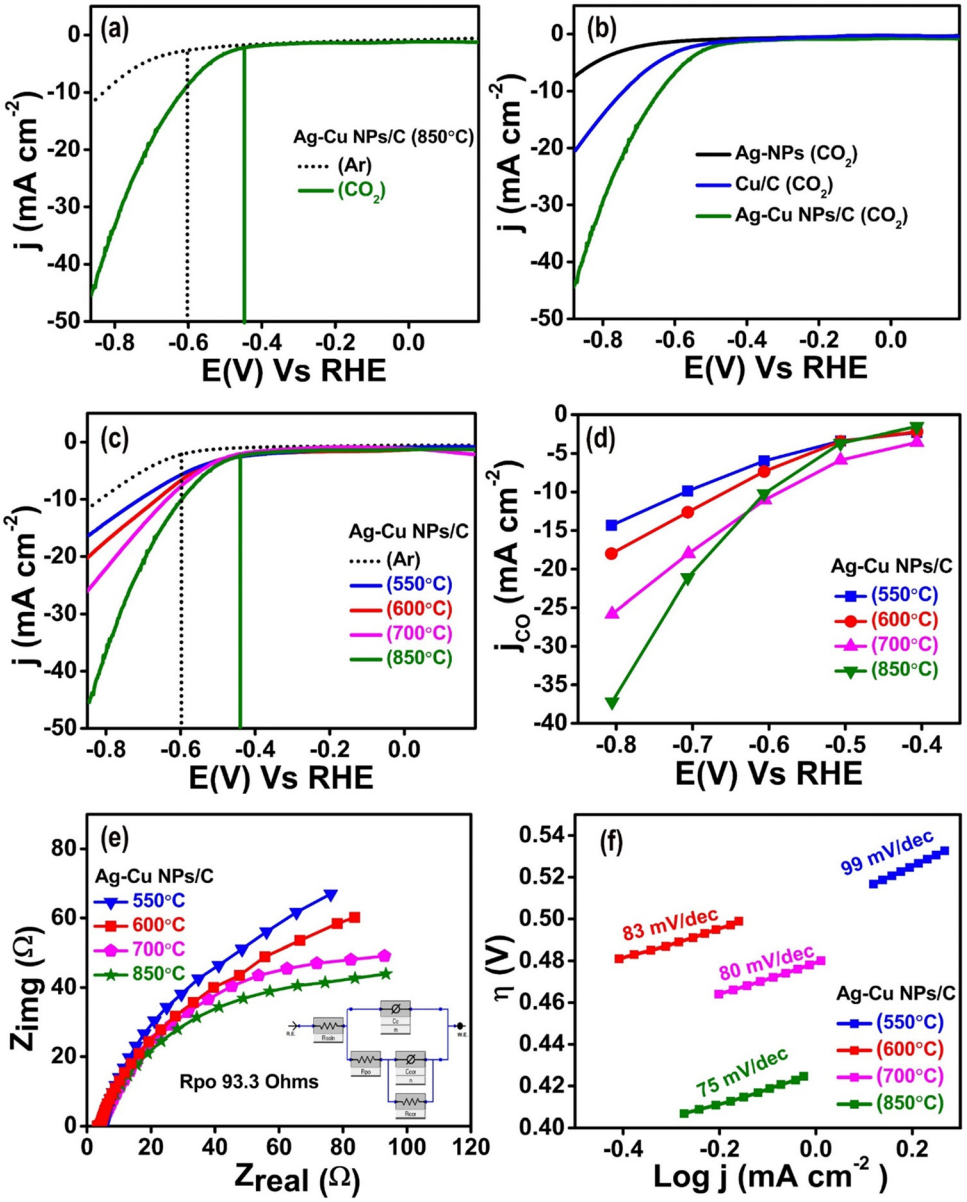

Fig. 2 Cathodic LSV results of (a) Ag–Cu NPs/C in Ar and CO_2 saturated solutions, (b) Ag-NPs, Cu/C and Ag–Cu NPs/C and (c) Ag–Cu NPs/C synthesized at different temperatures. (d) Partial CO (j_{CO}) of all the synthesized electrocatalysts. (e) EIS (Nyquist plot) of Ag–C at different temperatures. (f) Tafel plot of Ag–Cu NPs/C at different temperatures.

plotting Z_{real} *vs.* Z_{imag} components of the circuit are called the Nyquist plot. The Rpo value determined by fitting is 93.3 ohm for Ag–Cu NPs/C which is small and confirms the faster electron transfer at the interface, resulting in enhanced reduction performance of the eCO_2RR, with a smaller charge transfer resistance (R_{ct}). Comparing the impedance results of all the synthesized catalysts indicates that our optimum electrocatalyst, Ag–Cu NPs/C (850°), has the smallest resistance to charge transfer having a smaller semicircular diameter, which is attributed to the synergistic interaction of copper and silver (as illustrated in Fig. 2(e)).

Tafel slope analysis was carried out to obtain a mechanistic understanding of the eCO_2RR and to evaluate the charge transfer kinetics on the catalyst's surface. The Tafel slope (η *vs.* log$j$) is shown in Fig. 2(f). The catalyst material (Ag–Cu NPs/C 850 °C) shows a lower Tafel value of only 75 mV dec^{-1}. The comparatively low Tafel slope obtained for Ag–Cu NPs/C (850 °C) compared to all the synthesized electrocatalysts is attributed to the synergistic effect of Ag and Cu. The presence of copper modifies the d-band of silver and enhances the CO_2 reduction reaction's selectivity and activity.

Chronoamperometry (CA) is the continuous measurement of current over time at a fixed potential and is an essential component of electroanalytical techniques. To evaluate the stability of the catalyst material, long term controlled potential electrolysis (CPE) of the CO_2 reduction reaction was performed

© 2024 The Author(s). Published by the Royal Society of Chemistry

Open Access Article. Published on 06 August 2024. Downloaded on 1/20/2026 8:15:24 PM.
This article is licensed under a Creative Commons Attribution-NonCommercial 3.0 Unported Licence.

through CA at different potentials from −0.4 V_{RHE} to −0.8 V_{RHE}. In CPE studies, the working electrode is held at a constant potential (V), and the current *vs.* time response is recorded. The result of the durability test over 10 h for all potentials is shown in Fig. 3(a), which indicates no remarkable change in *j*, confirming that the optimum electrocatalyst Ag–Cu NPs/C 850 °C is stable enough, making it suitable for long time use in the reduction of CO_2. Moreover, the long term stability test of the optimum ratio at −0.79 V_{RHE} for 40 h showing only a 2% loss in activity is illustrated in Fig. S7 (ESI†). During the stability test, various parameters, such as catalytic activity, selectivity, and structural integrity, were monitored to ascertain any potential degradation or deactivation of the catalyst. The results indicated a consistent performance with a minimal loss in catalytic efficiency, thereby underscoring the robustness and reliability of the catalyst under continuous operational conditions.

Product analysis shows that carbon monoxide (CO) is the main gaseous product formed in the eCO_2RR. Gas chromatography (GC) was performed using helium as a carrier gas and the gas quantification was achieved by generating calibration curves from the standard of CO. The chromatogram shows peaks for CO_2 and CO, which were detected at distinct time intervals. The retention time (R_t) for CO_2 in the column was 5.3 min, while the R_t for CO was 7.4 min. After 1 h, a short peak of CO was observed; the intensity of the CO peak was increased after 2–10 h, while the intensity of the CO_2 peak decreased which confirms that some of the CO_2 actively participated in the reaction and converted to CO as

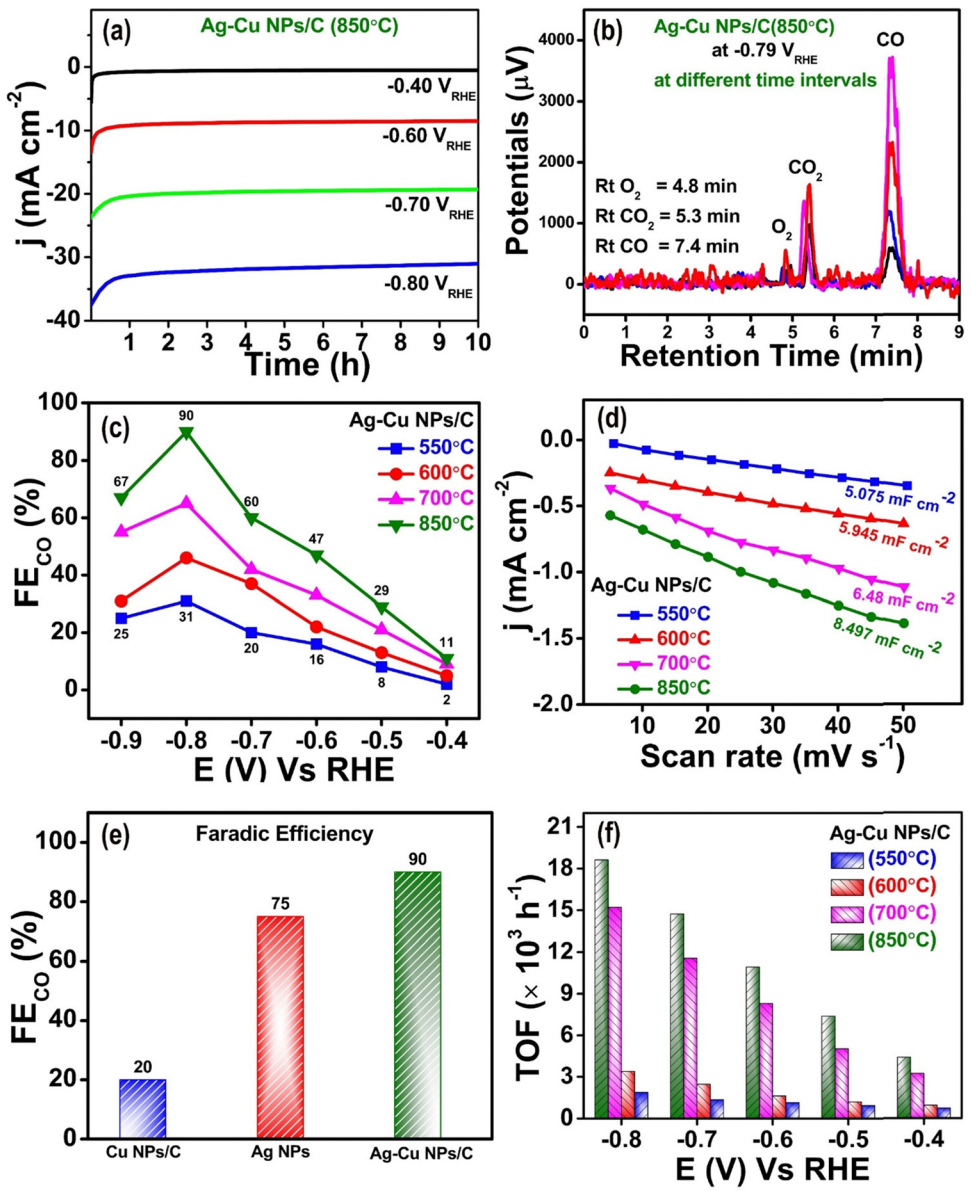

Fig. 3 (a) CA of Ag–Cu NPs/C 850 °C at different potentials over 10 h. (b) Gas chromatogram of Ag–Cu NPs/C 850 °C at −0.79 V_{RHE}. (c) FE_{CO}% at various applied potentials from −0.4 V_{RHE} to −0.9 V_{RHE}. (d) Linear Cdl plot of Ag–Cu NPs/C at different temperatures. (e) Comparative FE_{CO}% of Cu NPs/C, Ag NPs and Ag–Cu NPs/C. (f) TOF of Ag–Cu NPs/C at different temperatures.

© 2024 The Author(s). Published by the Royal Society of Chemistry

Open Access Article. Published on 06 August 2024. Downloaded on 1/20/2026 8:15:24 PM. This article is licensed under a Creative Commons Attribution-NonCommercial 3.0 Unported Licence.

Table 1 Comparison of previously reported Ag–Cu bimetallic catalysts with our work for the eCO_2RR

Catalyst	Electrolyte ($KHCO_3$) M	Electrolytic cell setup	Applied potential (V *vs.* RHE)	FE_{CO}%	Ref.
Ag–Cu NPs/C	**0.1**	**H-Cell**	**−0.79**	**90**	**This work**
$Ag_{83}Cu_{17}$	0.5	H-Cell	−1.10	74	53
Ag dendrites on Cu foam	0.5	Flow cell	−0.80	95.7	54
$Ag_{1.01\%}$/CuO	0.1	H-Cell	−0.70	91.2	55
Ag@Cu-7	0.1	H-Cell	−1.06	82	56
Cu/Ag layered	0.1	H-Cell	−0.80	89.1	57
$Ag_{96}Cu_4$	0.1	Flow cell	−1.0	98.7	58
$Ag_{84}Cu_{16}$ dendrite	0.5	H-Cell	−0.645	43.9	59
AgCu-50	0.1	H-Cell	−0.60	58.4	60
Ag/Cu NWs	0.5	H-Cell	−0.82	39.6	61
Spongeous $Ag_{91}Cu_9$	0.1	H-Cell	−0.70	80.6	62
$Ag_{88}Cu_{12}$ aerogel	0.1 M $NaHCO_3$	H-Cell	−0.89	89.40	63

illustrated in Fig. 3(b). The change in FE_{CO}% by using all the synthesized Ag–Cu NPs/C electrocatalysts at various potentials (from −0.4 V_{RHE} to −0.9 V_{RHE}) shows that the maximum FE_{CO}% is obtained at a potential of −0.79 V_{RHE}, which indicates that the selectivity of CO depends on the applied potential and is summarized in Fig. 3(c).

The change in FE_{CO}% of the optimum ratio of the synthesized electrocatalyst (Ag–Cu NPs/C 850 °C) was analyzed by performing the eCO_2RR at a fixed potential of −0.79 V_{RHE} with the continued bubbling of CO_2 for 10 h as shown in Fig. S3 (ESI†). As illustrated in Fig. 3(e), the electrocatalytic performance of Cu/C, Ag-NPs, and Ag–Cu NPs/C, the comparative FE_{CO}% graph shows that Ag–Cu NPs/C exhibits superior faradaic efficiency with a value of 90% than those of pure silver (75%) and copper (20%) metal. This indicates that the selectivity of the eCO_2RR to CO has been improved by combining Ag with MOF-derived Cu/C and can be controlled by adjusting the applied potential.

The electrochemically active surface area (ECSA) of the electrodes was measured using an electrical double-layer capacitance (C_{dl}) as an indicator to further explore how the electrode material influences electrocatalytic performance. Cyclic voltammetry (CV) was carried out in the non-faradaic region at various scan rates ranging from 5 to 50 mV s^{-1} as presented in Fig. S4(a)–(d) (ESI†). The straight line is obtained by plotting scanning rates against the corresponding current and the slope of the straight-line yields the C_{dl} value. The calculated C_{dl} values of 5.075 mF cm^{-2}, 5.945 mF cm^{-2}, 6.48 mF cm^{-2}, and 8.497 mF cm^{-2} for Ag–Cu NPs/C 550 °C, Ag–Cu NPs/C 600 °C, Ag–Cu NPs/C 700 °C, and Ag–Cu NPs/C 850 °C, respectively, are demonstrated in Fig. 3(d). By using the formula $\text{ECSA} = \frac{C_{dl}}{C_s}$ the ECSA was calculated, where C_s is the specific capacitance, and its value is 0.029 mF cm^{-2}. The maximum ECSA value obtained for Ag–Cu NPs/C 850 °C was 293 cm^2 as illustrated in Fig. S5 (ESI†). A catalyst with a larger value of the ESCA will possess more active sites thereby improving its performance for the eCO_2RR (high j and low η).

The turnover frequency (TOF) for CO_2 reduction was evaluated at various potentials between −0.4 V and −0.8 V (*vs.* RHE) in a CO_2-saturated medium to estimate the intrinsic performance of Ag and Cu active sites. The optimum electrocatalyst Ag–Cu NPs/C 850 °C gives a high TOF value of $\sim 19 \times 10^3$ h^{-1} at −0.8 V_{RHE}, much higher (14.6 times) than that of Ag–Cu NPs/C 550 °C ($\sim 1.30 \times 10^3$ h^{-1} at −0.8 V_{RHE}). The higher TOF value of Ag–Cu NPs/C 850 °C indicates a faster rate of the eCO_2RR to CO (as illustrated in Fig. 3(f)). Table 1 presents the comparative analysis of Ag–Cu based electrocatalysts with the recent literature.

Conclusions

In summary, we presented an Ag–Cu based bimetallic nanomaterial, Ag–Cu NPs/C, and evaluated its performance in the eCO_2RR to CO. Ag–Cu NPs/C was synthesized by the incorporation of silver nanoparticles into Cu-BTC metal organic frameworks and subsequent carbonization at higher temperature under a hydrogen environment. The as-prepared catalyst has shown high performance for the eCO_2RR, with a FE_{CO} value of ∼ 90% at −0.79 V_{RHE} and a j-value of 44.15 mA cm^{-2} at a low onset potential of 0.430 V_{RHE}. The stability test over 10 h also confirms the excellent performance of Ag–Cu NPs/C. The nanostructure, dispersion, and synergistic combination of silver and copper nanoparticles are responsible for accelerating the activity and selectivity for the conversion of CO_2 to CO. The results demonstrate the potential of this material for the development of sustainable CO_2 reduction technologies.

Data availability statement

The data underlying this study will be available upon request.

Conflicts of interest

There are no conflicts to declare.

Note added after first publication

This article replaces the version published on 6th August 2024, which contained errors in Scheme 1.

Open Access Article. Published on 06 August 2024. Downloaded on 1/20/2026 8:15:24 PM.
This article is licensed under a Creative Commons Attribution-NonCommercial 3.0 Unported Licence.

Acknowledgements

This work is supported by the Chinese Academy of Sciences (CAS) (2024PVA0016). MAN acknowledges the CAS for the grant of ''President's International Fellowship Initiative'' (PIFI) award.

References

1 M. Sturman and M. Oelgemöller, Process parameters in the electrochemical reduction of carbon dioxide to ethylene, *ChemBioEng Rev.*, 2021, **8**(3), 149–188.
2 S. Zhao, S. Li, T. Guo, S. Zhang, J. Wang, Y. Wu and Y. Chen, Advances in Sn-based catalysts for electrochemical CO_2 reduction, *Nano-Micro Lett.*, 2019, **11**(1), 1–19.
3 Y. Ye, Y. Liu, Z. Li, X. Zou, H. Wu and S. Lin, Highly selective and active Cu-In_2O_3/C nanocomposite for electrocatalytic reduction of CO_2 to CO, *J. Colloid Interface Sci.*, 2021, **586**, 528–537.
4 I. Merino-Garcia, J. Albo, P. Krzywda, G. Mul and A. Irabian, Bimetallic Cu-based hollow fibre electrodes for CO_2 electroreduction, *Catal. Today*, 2020, **346**, 34–39.
5 T. Van Phuc, S. G. Kang, J.-S. Chung and S. H. Hur, Highly selective metal-organic framework-based electrocatalyst for the electrochemical reduction of CO_2 to CO, *Mater. Res. Bull.*, 2021, **138**, 111228.
6 J. Albo, A. Sáez, J. Solla-Gullón, V. Montiel and A. Irabien, Production of methanol from CO2 electroreduction at Cu_2O and Cu_2O/ZnO-based electrodes in aqueous solution, *Appl. Catal., B*, 2015, **176**, 709–717.
7 J. Albo, G. Beobide, P. Castaño and A. Irabien, Methanol electrosynthesis from CO_2 at Cu_2O/ZnO propmted by pyridine-based aqueous solutions, *J. CO_2 Util.*, 2017, **18**, 164–172.
8 W. Ahmad, P. Koley, S. Dwivedi, R. Lakshman, Y. K. Shin, A. C. T. van Duin, A. Shrotri and A. Tanksale, Aqueous phase conversion of CO_2 into acetic acid over thermally transformed MIL-88B catalyst, *Nat. Commun.*, 2023, **14**, 2821.
9 M. Liu, Y. Pang, B. Zhang, P. De Luna, O. Voznyy, J. Xu, X. Zheng, C. T. Dinh, F. Fan and C. Cao, Enhanced electrocatalytic CO_2 reduction *via* field-induced reagent concentration, *Nature*, 2016, **537**(7620), 382–386.
10 D. Ren, N. T. Wong, A. D. Handoko, Y. Huang and B. S. Yeo, Mechanistic insights into the enhanced activity and stability of agglomerated Cu nanocrystals for the electrochemical reduction of carbon dioxide to n-propanol, *J. Phys. Chem. Lett.*, 2016, **7**(1), 20–24.
11 C.-T. Dinh., T. Burdyny, M. G. Kibria, A. Seifitokaldani, C. M. Gabardo, F. P. García de Arquer, A. Kiani, J. P. Edwards, P. De Luna, O. S. Bushuyev, C. Zou, R. Quintero-Bermudez, Y. Pang, D. Sinton and E. H. Sargent, CO_2 electroreduction to ethylene *via* hydroxide-mediated copper catalysis at an abrupt interface, *Science*, 2018, **360**(6390), 783–787.
12 I. Merino-Garcia, J. Albo, J. Solla-Gullón, V. Montiel and A. Irabian, Cu oxide/ZnO-based surfaces for a selective ethylene production from gas phase CO_2 electroconversion, *J. CO_2 Util.*, 2019, **31**, 135–142.
13 J. Shan, Y. Shi, H. Li, Z. Chen, Y. Shuai and Z. Wang, Effective CO_2 electroreduction toward C_2H_4 boosted by Ce-doped Cu nanoparticles, *Chem. Eng. J.*, 2022, **433**, 133769.
14 S. Zhang, Q. Fan, R. Xia and T. J. Meyer, CO_2 reduction from homogeneous to heterogeneous electrocatalysis, *Acc. Chem. Res.*, 2020, **53**(1), 255–264.
15 J. Wang, X. Huang, S. Xi, J. M. Lee, C. Wang, Y. Du and X. Wang, Linkage effect in the heterogenization of cobalt complexes by doped graphene for electrocatalytic CO_2 reduction, *Angew. Chem., Int. Ed.*, 2019, **58**(38), 13532–13539.
16 J. Albo, M. Perfecto-Irigaray, G. Beobide and A. Irabian, Cu/Bi metal-organic framework-based systems for an enhanced electrochemical transformation of CO_2 to alcohol, *J. CO_2 Util.*, 2019, **33**, 157–165.
17 A. Goyal, G. Marcandalli, V. A. Mints and M. T. Koper, Competition between CO_2 reduction and hydrogen evolution on a gold electrode under well-defined mass transport conditions, *J. Am. Chem. Soc.*, 2020, **142**, 4154–4161.
18 J. F. Xie, J. J. Chen, Y. X. Huang, X. Zhang, W. K. Wang, G. X. Huang and H. Q. Yu, Selective electrochemical CO_2 reduction on Cu-Pd heterostructure, *Appl. Catal., B*, 2020, **270**, 118864.
19 C. Chen, Z. Zhang, G. Li, L. Li and Z. Lin, Recent advances on nanomaterials for electrocatalytic CO_2 conversion, *Energy Fuels*, 2021, **35**(9), 7485–7510.
20 S. Gong, W. Wang, X. Xiao, J. Liu, C. Wu and X. Lv, Elucidating influence of the existence formation of anchored cobalt phthalocyanine on electrocatalytic CO_2-to-CO conversion, *Nano Energy*, 2021, **84**, 105904.
21 C. A. Trickett, A. Helal, B. A. Al-Maythalony, Z. H. Yamani, K. E. Cordova and O. M. Yaghi, The chemistry of metal-organic frameworks for CO_2 capture, regeneration and conversion, *Nat. Rev. Mater.*, 2017, **2**, 17045.
22 M. S. Lohse and T. Bein, Covalent organic frameworks: structures, synthesis, and applications, *Adv. Funct. Mater.*, 2018, **28**, 1705553.
23 Q. Wu, J. Liang, J. D. Yi, D. L. Meng, P. C. Shi, Y. B. Huang and R. Cao, Unraveling the relationship between the morphologies of metal–organic frameworks and the properties of their derived carbon materials, *Dalton Trans.*, 2019, **48**(21), 7211–7217.
24 A. Han, B. Wang, A. Kumar, Y. Qin, J. Jin, X. Wang, C. Yang, B. Dong, Y. Jia and J. Liu, Recent advances for MOF-derived carbon-supported single-atom catalysts, *Small Methods*, 2019, **3**(9), 1800471.
25 W. Yang, X. Li, Y. Li, R. Zhu and H. Pang, Applications of metal–organic-framework-derived carbon materials, *Adv. Mater.*, 2019, **31**(6), 1804740.
26 M. Perfecto-Irigaray, J. Albo, G. Beobide, O. Castillo, A. Irabian and S. Pérez-Yáñez, Synthesis of heterometallic metal-organic frameworks and their performance as electrocatalyst for CO_2 reduction, *RCS Adv.*, 2018, **8**(38), 21092.
27 K. Shen, X. Chen, J. Chen and Y. Li, Development of MOF-derived carbon-based nanomaterials for efficient catalysis, *ACS Catal.*, 2016, **6**, 5887–5903.

© 2024 The Author(s). Published by the Royal Society of Chemistry

Open Access Article. Published on 06 August 2024. Downloaded on 1/20/2026 8:15:24 PM. This article is licensed under a Creative Commons Attribution-NonCommercial 3.0 Unported Licence.

28 Y. F. Zhang, C. Yu, X. Y. Tan, S. Cui, W. B. Li and J. S. Qiu, Recent advances in multilevel nickel-nitrogen-carbon catalysts for CO_2 electroreduction to CO, *New Carbon Mater.*, 2021, **36**, 19–33.

29 C. Zhao, X. Dai, T. Yao, W. Chen, X. Wang, J. Wang, J. Yang, S. Wei, Y. Wu and Y. Li, Ionic exchange of metal-organic frameworks to access single nickel sites for efficient electroreduction of CO_2, *J. Am. Chem. Soc.*, 2017, **139**(24), 8078–8081.

30 H. Liu, J. Liu and B. Yang, Computational insights into the strain effect on the electrocatalytic reduction of CO_2 to CO on Pd surfaces, *Phys. Chem. Chem. Phys.*, 2020, **22**(17), 9600–9606.

31 S. Gao, Y. Lin, X. Jiao, Y. Sun, Q. Luo, W. Zhang, D. Li, J. Yang and Y. Xie, Partially oxidized atomic cobalt layers for carbon dioxide electroreduction to liquid fuel, *Nature*, 2016, **529**(7584), 68–71.

32 L. Yan, W. Su, X. Cao, P. Zhang and Y. Fan, Copper-indium hybrid derived from indium-based metal-organic frameworks grown on oxidized copper foils promotes the efficient electroreduction of CO_2 to CO, *Chem. Eng. J.*, 2021, **412**, 128728.

33 S. P. Liu, Y. Wang and S. Norwood, Discovering effective descriptors for CO_2 electroreduction to predict the catalysts with different selectivity, *J. Phys. Chem. C*, 2021, **125**, 4550–4558.

34 S. Gul, F. Nasim, W. Iqbal, A. Waseem and M. A. Nadeem, High performance electrochemical CO_2 reduction over Pd decorated cobalt containing nitrogen doped carbon, *RSC Adv.*, 2024, **14**(19), 13017–13026.

35 Z. Tian, C. Priest and L. Chen, Recent progress in the theoretical investigation of electrocatalytic reduction of CO_2. Adv, *Theory Simul.*, 2018, **1**(5), 1800004.

36 Y. Wang, C. Niu and Y. Zhu, Copper–silver bimetallic nanowire arrays for electrochemical reduction of carbon dioxide, *Nanomaterials*, 2019, **9**(2), 173.

37 D. Kim, J. Resasco, Y. Yu, A. M. Asiri and P. Yang, Synergistic geometric and electronic effects for electrochemical reduction of carbon dioxide using gold–copper bimetallic nanoparticles, *Nat. Commun.*, 2014, **5**(1), 1–8.

38 H. Liu, Y. Zhu, J. Ma, Z. Zhang and W. Hu, Recent advances in atomic-level engineering of nanostructured catalysts for electrochemical CO_2 reduction, *Adv. Funct. Mater.*, 2020, **30**(17), 1910534.

39 Y.-F. Zhang, C. Yu, X.-Y. Tan, S. Cui, W.-B. Li and J.-S. Qiu, Recent advances in multilevel nickel–nitrogen–carbon catalysts for CO_2 electroreduction to CO, *New Carbon Mater.*, 2021, **36**(1), 19–33.

40 Q. Dou, Y. Li, K. W. Wong and K. M. Ng, Facile synthesis of nearly monodisperse AgCu alloy nanoparticles with synergistic effect against oxidation and electromigration, *J. Mater. Res.*, 2019, **34**(12), 2095–2104.

41 J. Resasco and A. T. Bell, Electrocatalytic CO_2 reduction to fuels: progress and opportunities, *Trends Chem.*, 2020, **2**(9), 825–836.

42 A. Vasileff, C. Xu, Y. Jiao, Y. Zheng and S. Z. Qiao, Surface and interface engineering in copper-based bimetallic materials for selective CO_2 electroreduction, *Chem*, 2018, **4**(8), 1809–1831.

43 F. Mattarozzi, N. Van Der Willige, V. Gulino, C. Keijzer, R. C. Van de Poll, E. J. Hensen and P. E. De Jongh, Oxide-derived silver nanowires for CO_2 electrocatalytic reduction to CO, *ChemCatChem*, 2023, **15**(22), e202300792.

44 M. Balamurugan, J. H. Jang, J. E. Kim, W. I. Choi, Y. I. Jo, S. Park, E. Varathan and K. T. Nam, Tuning the CO_2 reduction selectivity of an immobilized molecular Ag complex beyond CO, *Inorg. Chem.*, 2024, **63**, 7992–8000.

45 M. Yang, J. Wu, Y. Li, H. Pan, H. Cui, X. Lu and X. Tang, Structural evolution of oxide-derived nanostructured silver electrocatalysts during CO_2 electroreduction, *ACS Catal.*, 2024, **14**(8), 6169–6178.

46 Z. Ma, T. Wan, D. Zhang, J. A. Yuwono, C. Tsounis, J. Jiang and R. Amal, Atomically dispersed Cu catalysts on sulfide-derived defective Ag nanowires for electrochemical CO_2 reduction, *ACS Nano*, 2023, **17**(3), 2387–2398.

47 Z. Zhang, S. Li, Y. Rao, L. Yang, W. Yan and H. Xu, Three-dimension porous Zn-Cu alloy: An inexpensive electrocatalyst for highly selective CO_2 reduction to CO in non-aqueous electrolyte, *J. Chem. Eng.*, 2024, **479**, 147376.

48 C. Du, J. P. Mills, A. G. Yohannes, W. Wei, L. Wang, S. Lu and Y. A. Wu, Cascade electrocatalysis *via* AgCu single-atom alloy and Ag nanoparticles in CO_2 electroreduction toward multicarbon products, *Nat. Commun.*, 2023, **14**(1), 6142.

49 H. A. Chaliyawala, S. Bastide, D. Muller-Bouvet, C. Pichon, K. Bah, A. Djoumoi and E. Torralba, One-Step Synthesis of Ag–Cu Bimetallic Nanoparticles on p-Si Photoelectrodes for Solar-Driven CO_2 Reduction, *ACS Appl. Energy Mater.*, 2023, **6**(16), 8397–8409.

50 T. Zhang, Y. Liu, C. Yang, L. Tian, Y. Yan and G. Wang, Monotonically increasing relationship between conversion selectivity from CO_2 to CO and the interface area of Cu–Ag biphasic electrochemical catalyst, *J. Alloys Compd.*, 2023, **947**, 169638.

51 W. Ye, X. Guo and T. Ma, A review on electrochemical synthesized copper-based catalysts for electrochemical reduction of CO_2 to C_2^+ products, *J. Chem. Eng.*, 2021, **414**, 128825.

52 A. Vishnyakov, P. I. Ravikovitch, A. V. Neimark, M. Bülow and Q. M. Wang, Nanopore structure and sorption properties of Cu–BTC metal–organic framework, *Nano Lett.*, 2003, **3**(6), 713–718.

53 D. Wei, Y. Wang, C. L. Dong, Z. Zhang, X. Wang, Y. C. Huang, Y. Shi, X. Zhao, J. Wang and R. Long, Decrypting the controlled product selectivity over Ag–Cu bimetallic surface alloys for electrochemical CO_2 reduction, *Angew. Chem., Int. Ed.*, 2023, **135**(19), e202217369.

54 F. l Urbain, P. Tang, N. M. Carretero, T. Andreu, J. Arbiol and J. R. Morante, Tailoring copper foam with silver dendrite catalysts for highly selective carbon dioxide conversion into carbon monoxide, *ACS Appl. Mater. Interfaces*, 2018, **10**(50), 43650–43660.

55 W. Zhang, N. Zhu, L. Ding, Y. Hu and Z. Wu, Efficacious CO_2 adsorption and activation on Ag nanoparticles/CuO

Open Access Article. Published on 06 August 2024. Downloaded on 1/20/2026 8:15:24 PM.
This article is licensed under a Creative Commons Attribution-NonCommercial 3.0 Unported Licence.

mesoporous nanosheets heterostructure for CO_2 electroreduction to CO, *Inorg. Chem.*, 2021, **60**(24), 19356–19364.

56 Z. Chang, S. Huo, W. Zhang, J. Fang and H. Wang, The tunable and highly selective reduction products on Ag@Cu bimetallic catalysts toward CO_2 electrochemical reduction reaction, *J. Phys. Chem. C*, 2017, **121**(21), 11368–11379.

57 W. J. Dong, C. J. Yoo, J. W. Lim, J. Y. Park, K. Kim, S. Kim, D. Lee and J.-L. Lee, Tailoring electronic structure of bifunctional Cu/Ag layered electrocatalysts for selective CO_2 reduction to CO and CH_4, *Nano Energy*, 2020, **78**, 105168.

58 M. Li, Y. Hu, G. Dong, T. Wu and D. Geng, Achieving tunable selectivity and activity of CO_2 electroreduction to CO *via* bimetallic silver–copper electronic engineering, *Small*, 2023, **19**(15), 2207242.

59 J. Choi, M. J. Kim, S. H. Ahn, I. Choi, J. H. Jang, Y. S. Ham, J. J. Kim and S.-K. Kim, Electrochemical CO_2 reduction to CO on dendritic Ag–Cu electrocatalysts prepared by electrodeposition, *J. Chem. Eng.*, 2016, **299**, 37–44.

60 T. Kottakkat, K. Klingan, S. Jiang, Z. P. Jovanov, V. H. Davies, G. A. El-Nagar, H. Dau and C. Roth, Electrodeposited AgCu foam catalysts for enhanced reduction of CO_2 to CO, *ACS Appl. Mater. Interfaces*, 2019, **11**(16), 14734–14744.

61 Y. Jeon, I. Choi and J. J. Kim, Facile electrochemical fabrication of Ag/Cu bi-metallic catalysts and the dependence of their selectivity for electrochemical CO_2 reduction on the surface composition, *Thin Solid Films*, 2021, **726**, 138674.

62 W. Zhang, C. Xu, Y. Hu, S. Yang, L. Ma, L. Wang, P. Zhao, C. Wang, J. Ma and Z. Jin, Electronic and geometric structure engineering of bicontinuous porous Ag–Cu nanoarchitectures for realizing selectivity-tunable electrochemical CO_2 reduction, *Nano Energy*, 2020, **73**, 104796.

63 W. Wang, S. Gong, J. Liu, Y. Ge, J. Wang and X. Lv, Ag–Cu aerogel for electrochemical CO_2 conversion to CO, *J. Colloid Interface Sci.*, 2021, **595**, 159–167.

© 2024 The Author(s). Published by the Royal Society of Chemistry